Thin-Walled Structures 179 (2022) 109677

Contents lists available at ScienceDirect

Thin-Walled Structures

journal homepage: www.elsevier.com/locate/tws

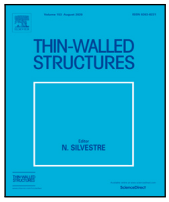

Full length article

Crashworthiness of foam filled truncated conical sandwich shells with corrugated cores

Mao Yang [a], Bin Han [b,*], Yongjian Mao [a], Jun Zhang [a], Tian Jian Lu [c,d,*]

[a] Institute of Systems Engineering, China Academy of Engineering Physics, Mianyang, 621999, PR China
[b] School of Mechanical Engineering, Xi'an Jiaotong University, Xi'an 710049, PR China
[c] State Key Laboratory of Mechanics and Control of Mechanical Structures, Nanjing University of Aeronautics and Astronautics, Nanjing 210016, PR China
[d] MIIT Key Laboratory of Multi-functional Lightweight Materials and Structures, Nanjing University of Aeronautics and Astronautics, Nanjing 210016, PR China

ARTICLE INFO

Keywords:
Energy absorption
Axial compression
Foam filling
Conical sandwich shell

ABSTRACT

Polymeric foam filled truncated metallic conical sandwich shells with corrugated cores were proposed, and their energy absorption characteristics under axial compression were systematically investigated. The types of foam filling include: (i) foam filling inner cavity (FFIC), (ii) foam filling corrugated channel (FFCC), and (iii) foam filling inner cavity and corrugated channel (FFICCC). Test specimens were fabricated by combining the step-by-step molding method with the method of in-situ foam filling. Firstly, the crashworthiness of FFIC, FFCC and FFICCC subjected to axial compression was experimentally characterized. Secondly, numerical simulations with the method of finite elements (FE) were performed, with good agreement achieved between measurements and simulations. Subsequently, based upon the validated FE models, interaction mechanisms between foam filler and metallic shell were explored, and the influences of wall thickness, semi-apical angle and loading speed on energy absorption were quantified. The three different foam filled structures were found to exhibit higher energy absorption than their unfilled counterpart. Particularly, the specific energy absorption (*SEA*) of the FFCC was higher than that of the unfilled structure, attributed mainly to the participation of all foam fillers in the interaction with metal shells that was rarely found in other types of foam-filled structure.

1. Introductions

The rapid development of advanced transportation vehicles in aviation, navigation and other fields led to increasing research efforts on their safety and crashworthiness. Although thin-walled metal tubes have been extensively exploited as energy absorption devices for transportation vehicles [1], the hunt for lighter and more efficient energy-absorbing structures remains a pressing necessity. For instance, metal tubes with various cross-sectional forms, such as cylindrical [2,3], square [4], triangular [5], rectangular [6], and multi-corner [7,8], were extensively studied as energy absorbers. In addition, compared with straight tubes, it had been demonstrated that tapered tubes had higher *SEA* (specific energy absorption, i.e., energy absorption per unit mass) and lower *PF* (peak force), more stable and controllable deformation, and better designability [9,10]. More recently, multi-celled tubes [11–13] and foam filled tubes [14–17] were also proposed for enhanced crashworthiness.

It has been demonstrated that the energy absorption (*EA*) capacity of a metal tube can be significantly enhanced by using the technique of foam filling. High porosity cellular aluminum (Al) foams and polyurethane (PU) foams have been commonly used as the filling material, due mainly to the following attributes: (a) Lightweight, for the porosity of a foam is typically high (>80%) and can even reach 99% [18]; (b) The foam exhibits an obvious plateau stress as it is crushed, i.e., the stress in the plastic deformation stage of its stress versus strain curve remains practically constant [19]; (c) The foam can realize a crushing force efficiency close to 1. Nonetheless, the foam typically has a low mean crushing force such that its total energy absorption is also small, thus requiring a large volume of foam material to achieve energy absorption under severe collision. To address this critical issue, it has been proposed to fill a thin-walled metal tube with the foam for enhanced *EA*, as this may not only take advantage of the high energy absorption characteristics of the metal tube and solve the problem of low total energy absorption of individual foam, but also exploit the interaction effect between the tube wall and the foam. Nonetheless, it had been found that foam filling could indeed lead to significantly enhanced *EA*, but the *SEA* was barely improved, since the structural mass was increased by foam filling. Therefore, how to efficiently design the style of foam filling to maximize the interaction effect and achieve enhancement in terms of both *EA* and *SEA* has become a critical issue for foam filled tubes.

* Corresponding authors.
E-mail addresses: hanbinghost@xjtu.edu.cn (B. Han), tjlu@nuaa.edu.cn (T.J. Lu).

https://doi.org/10.1016/j.tws.2022.109677
Received 7 February 2022; Received in revised form 19 June 2022; Accepted 19 June 2022
Available online xxxx

At present, several new fillers based on cellular and porous solid materials, in particular cellular metals (e.g. closed aluminum foams, polymer-open cell aluminum foams and metal hollow spheres) for preparing filled tubular structures have been developed and studied [20–25]. However, the few existing studies on foam filled tubes mainly concerned filling relatively simple structures, and the filling was mainly filled in a large space of the tube structure. For instance, polyurethane foam was used to fill a thin-walled conical shell to improve its crush energy absorption capability [26]. It was discovered that for a tube with thicker wall, in comparison to its empty counterpart, foam filling had minimal influence on its energy absorption; however, under oblique loading, the foam filled tube exhibited better crashworthiness. Similarly, filling a corrugated tube with foam led to elevated *EA* of the hybrid structure, but not the *SEA* and, the smaller the density of foam, the more the reduction in *SEA* [27]. In addition, foam filling was found to increase the *CFE* of the structure, and the smaller the foam density, the more the increase in *CFE*. Yao et al. [28] investigated the crashworthiness of aluminum foam-filled grooved tube under axial compression, and achieved similar conclusions: the foam filled tube exhibited a larger mean crushing force and *CFE* than the empty tube, but a lower *SEA*. In the foam filled tubes mentioned above, the low *SEA* was mainly attributed to the small contact area between the foam and metal tube, such that the interaction effect between the two was not strong. Subsequently, based upon numerical simulations, filling a multi-tubular circular tube with foam was found to effectively increase the contact area between the foam and tube, and hence the foam filled structure acquired a higher *SEA* than its empty counterpart [29]. However, due to the complexity of fabrication for such structures, the corresponding experimental research was lacking. In response to the difficulty in the fabrication of foam filled complex structures, the filling method of in-situ foaming was proposed [30]. This method enables filling complex structures with polymer foams, thus providing a good choice for the preparation of foam filled structures. However, there was almost no research on applying this preparation method to complex tubular structures for energy absorption applications.

In addition to conventional metal tubes with monolithic walls, tubes with sandwich walls have also been envisioned as high-performance energy absorbers. In particular, sandwich structures with fluid-through cellular cores have been extensively studied due mainly to ultra-lightweight, high specific stiffness/strength, and high *SEA* [31–34]. In recent years, other attributes of these highly porous sandwich structures have also been exploited, such as good fillability and designability, thus enabling multifunctionality. For instance, upon filling the interstices of the sandwich core with foam [35,36], honeycomb [37], water [38], sand [39], ceramic [40] and other materials, the hybrid-cored sandwich exhibits better single performance or multi-functional characteristics, such as active heat dissipation, sound absorption, and blast/penetration resistance. However, existing research on such novel sandwich constructions was mainly about plates and beams, with much less research on sandwich-walled tubes. Recently, with focus placed upon applying sandwich construction to energy absorbing tubes, the present authors [41–44] proposed a truncated conical sandwich shell with corrugated core (TCSS) and conducted a detailed study on its energy absorption performance using a combined experimental, analytical and numerical approach. It was demonstrated that the novel TCSS exhibited excellent crashworthiness. However, at present, how foam filling would affect the crashworthiness of such sandwich tubular structures remains elusive. This issue is addressed in the present study, both experimentally and numerically.

Three different types of foam filled metallic truncated conical sandwich shell with corrugated core were proposed: (i) foam filling inner cavity (FFIC), (ii) foam filling corrugated channel (FFCC), and (iii) foam filling inner cavity and corrugated channel (FFICCC). Test specimens were prepared using a combination of the step-by-step molding method and the in-situ foam filling approach. Energy absorption behaviors of the specimens under axial compression were experimentally characterized. Numerical simulations with the method of finite elements (FE) to explore further the underlying physical mechanisms and the influence of different foam filled constructions. Strengthening mechanisms, parametric influences, and dynamic loading were also analyzed based on FE simulations.

Table 1
Geometric parameters of TCSS specimens.

t (mm)	R_{i-u} (mm)	R_{o-u} (mm)	R_{i-d} (mm)	R_{o-d} (mm)	w (mm)	θ (°)	Height (mm)	α (°)
0.2	57.7	66.7	95.0	104.9	2.0	14.9	145.0	18

2. Experiment

2.1. Materials and specimen preparation

Truncated conical sandwich shells with corrugated cores (TCSS) were fabricated via a step-by-step molding process, with geometrical dimensions as illustrated in Fig. 1 and Table 1. Aluminum alloy 1060Al was selected as the parent material of all the TCSS structures fabricated. Detailed fabrication process had been described in a previous work [41] and hence was omitted here for brevity.

To enhance further the energy absorption capability of the already excellent energy absorbing TCSS structures, the liquid self-foaming PU foam was selected as the foam filler, for it could be conveniently foamed in-situ in complex voids or channels. Preparation of the PU foam was illustrated schematically in Fig. 2: the two preformed liquids A and B were fully mixed, and then poured into a prebuilt mold; subsequently, polymerization reaction between the diisocyanate and polylo was initiated, which caused rapid solidification of the mixture, thus producing the in-situ PU foam.

Based on the in-situ foaming technique, Fig. 3 presented the basic filling scheme to construct the three different foam-filled TCSS structures proposed by the present study: (i) foam filling inner cavity (FFIC), (ii) foam filling corrugated channel (FFCC), and (iii) foam filling inner cavity and corrugated channel (FFICCC).

2.2. Axial crushing tests

Quasi-static compression tests of as-fabricated foam filled TCSS specimens were carried out with a hydraulic testing machine (maximum load: ±100 kN, maximum displacement: ±100 mm). As shown in Fig. 4, the bottom platen was fixed, the upper platen only moved along the axial direction, and the specimen was freely placed between the upper and bottom platens. The upper platen moved downward with a speed of 1 mm/min, and the maximum compression distance was fixed at 50 mm. Both the displacement and compressive force were recorded by the signal acquisition system.

2.3. Compression characteristics (crashworthiness)

To evaluate the crashworthiness of an energy-absorbing structure, relevant parameters include [45]: total absorbed energy (*EA*), specific energy absorption (*SEA*), peak force (*PF*), specific energy absorption per unit volume (*SEAV*). In the field of vehicle collision, an energy-absorbing structure is said to have good crashworthiness if it exhibits high *EA*, *SEA*, *SEAV* and low *PF* [9]. Desired parameters in this research which are used could be obtained from load–displacement curve are as follows:

2.3.1. Total absorbed energy (EA)

The total energy absorption *EA*, which describes the energy absorption capacity of each pair of specimens, is defined as the integration of the force vs. deformation curve:

$$EA = \int_0^{\delta} F(x)dx$$

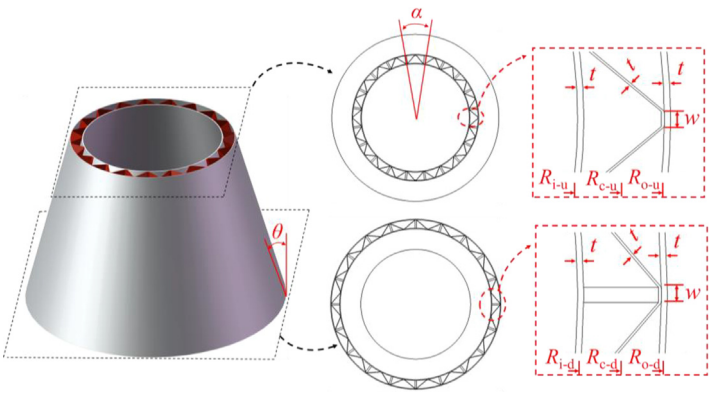

Fig. 1. Geometric parameters of truncated conical sandwich shell with corrugated core.

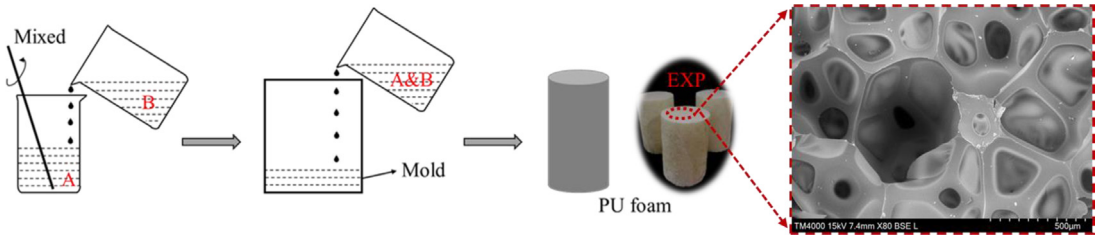

Fig. 2. Preparation of PU foam.

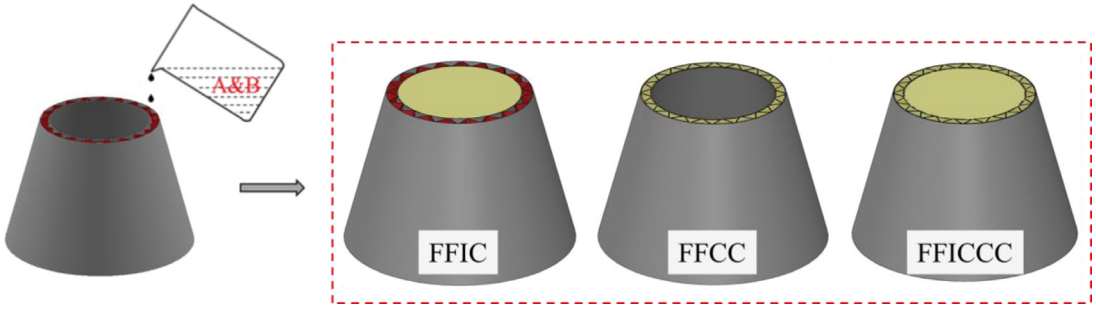

Fig. 3. Preparation of foam filled TCSS with varying filling approach, including foam filling inner cavity (FFIC), foam filling corrugated channel (FFCC), and foam filling inner cavity and corrugated channel (FFICCC).

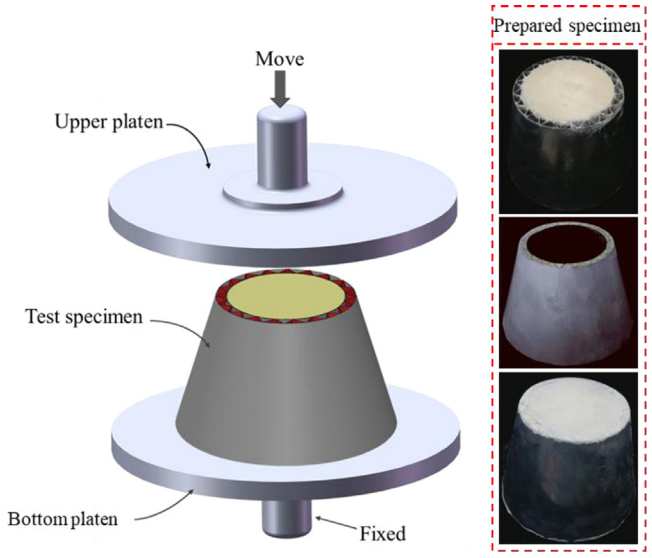

Fig. 4. Schematic of a foam filled TCSS specimen under axial compression. Right side presented photos of as-fabricated FFIC (upper) and FFICCC (bottom) specimens.

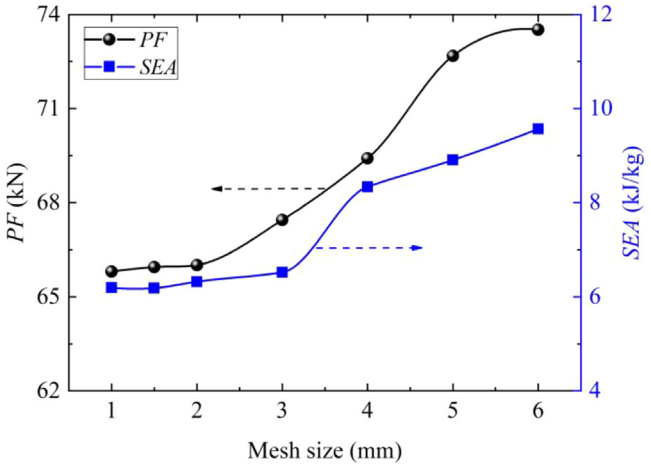

Fig. 5. Mesh sensitivity of the *PF* and *SEA*.

where $F(x)$ is the crushing force as a function of crush distance x, and δ is the axial crushing distance.

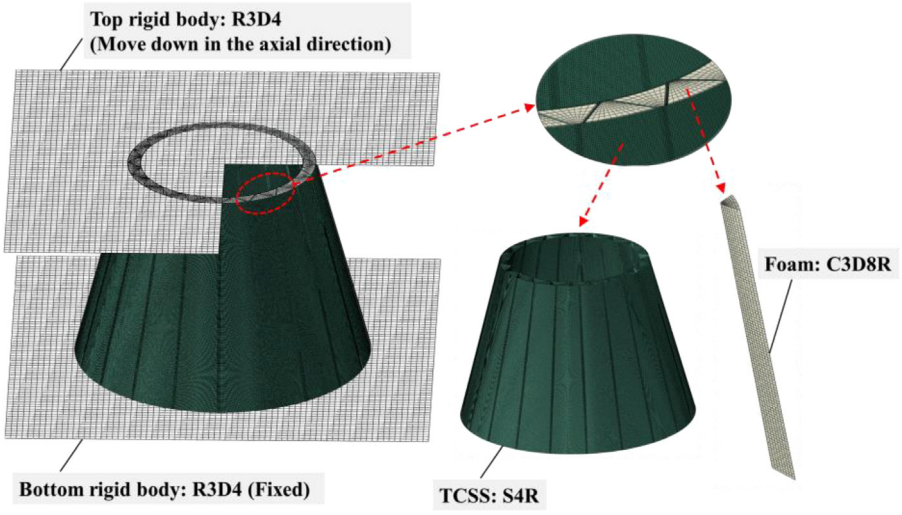

Fig. 6. Finite element model and related settings.

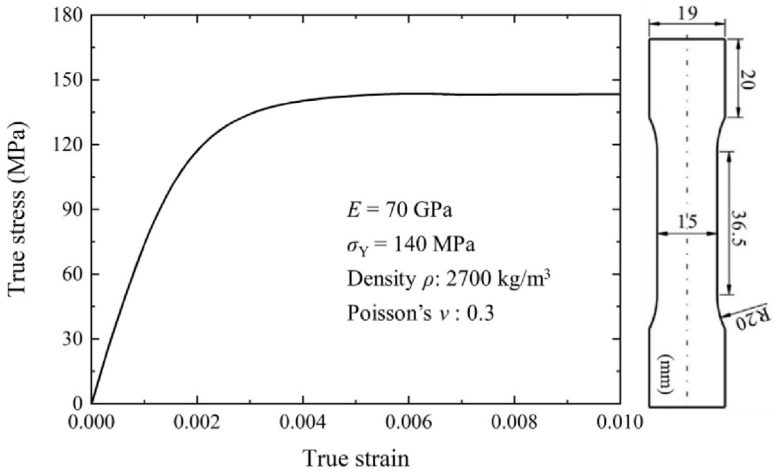

Fig. 7. True stress versus true strain curve of 1060Al obtained via quasi-static uniaxial tension based on ISO6892-1.

2.3.2. The specific energy absorption (SEA)

The specific energy absorption, *SEA*, which is defined as the energy absorbed per unit mass, provides a way of comparing energy absorption capacity of structures with different masses and is given by:

$$SEA = \frac{EA}{m} \tag{1}$$

where m is the total mass of the pair of specimens.

2.3.3. Mean crushing force (MCF)

One of the most significant parameters for quantifying the behavior of axially compressed tubes is the mean crushing force, which is obtained by dividing the measured absorbed energy to the total crushing distance δ:

$$MCF = \frac{EA}{\delta} \tag{2}$$

2.3.4. Specific energy absorption per unit volume (SEAV)

The specific energy absorption per unit volume, *SEAV*, which is defined as the energy absorbed per unit volume:

$$SEAV = \frac{EA}{V} \tag{3}$$

where V is the volume of the energy absorber. The *SEAV* often used for sandwich structures.

3. Finite element modeling

3.1. FE model

Foam filled TCSS specimens under quasi-static axial compression were simulated using the nonlinear explicit FE algorithm ABAQUS/Explicit. The FE model developed was shown in Fig. 5, in which two rigid bodies were used to simulate the upper and bottom platens of the experiment. The upper rigid body slid downward in the axial direction, whereas the bottom rigid body was fully stationary. The compression distance, 50 mm, was identical to that adopted in the experiment.

The FE model could be divided into three parts, i.e., the all-metallic truncated conical sandwich shell (TCSS), the foam fillers, and the upper and bottom rigid bodies. General contact was defined throughout the FE model, and the coefficient of friction was set as 0.2 [41,46,47]. The TCSS was all modeled using the S4R element, with 5-integration points through the thickness, this element formulation gives greater computational efficiency compared to other element formulations [48], the foam fillers were modeled with the eight-node solid elements (C3D8R), while the upper and lower rigid bodies were modeled using four-node rigid elements (R3D4). Upon checking the convergence of numerical solutions, the optimal mesh size for the TCSS and foam fillers were selected as 1.5 × 1.5 mm and 2 × 2 mm, respectively. For instance, Fig. 5 depicts the *PF* and *SEA* of the TCSS under quasi-static axial

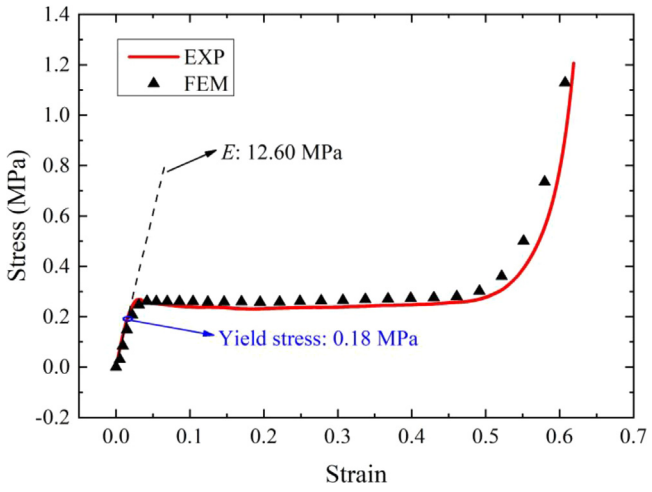

Fig. 8. Quasi-static uniaxial compressive stress versus strain curve of PU foam: comparison between experiment and FE simulation.

Table 2
Material parameters of crushable foam model for PU foam.

Density (kg/m^3)	Elastic modulus (MPa)	Poisson ratio [26]	Compression yield stress ratio [26]	Plastic Poisson ratio [26]
41	12.60	0	1	0

loading as a function of mesh size. It was evident from the graph that a 1.5 mm mesh size can produce accurate results. Similar graphs were obtained for other foam filled TCSS tubes that were not reported here for the sake of brevity.

The material of the present TCSS was 1060Al. The material properties were tested in accordance with standard: ISO6892-1. The stress–strain curve obtained from quasi-static uniaxial tensile test of 1060Al, together with its fundamental mechanical properties, showed in Fig. 7. In the FE simulation, the stress–strain curve was used as the material property, and the isotropic hardening model was employed. The foam filling was described using an isotropic crushable foam material model, the stress–strain curve was used as the material property, shown in Fig. 8; other foam properties adopted in the FE simulation were listed in Table 2. For validation, the numerically calculated stress versus strain curve (marked by black triangles) was checked against that measured experimentally (marked as red line), as shown in Fig. 8. It was seen that the present numerical simulation of the foam material was accurate (see Fig. 6).

3.2. Validation against experimental measurements

Fig. 9 compared the experimentally measured force versus displacement curves and deformation modes of FFIC, FFCC, and FFICCC under quasi-static axial compression with those numerically simulated, whereas Table 3 listed the key evaluative indicators, i.e., *PF*, *EA* and *SEA*. The force versus displacement curve exhibited large reciprocating fluctuations, induced by the continuous formation of plastic hinges [41]. The FE simulations agreed well with experiments in terms of both force versus displacement curves and deformation modes. However, there was a certain error between the finite element results and the experimental results. The experimental curves were albeit slightly lower than the simulated ones, mainly attributed to the presence of various defects (*e.g.*, pits, degumming, and initial buckling) induced during the fabrication process of the TCSS [41]. In addition, at the beginning of the compression experiment, the indenter and the specimen were not completely fitted at the beginning, but in the finite element model, the indenter and the specimen were completely fitted.

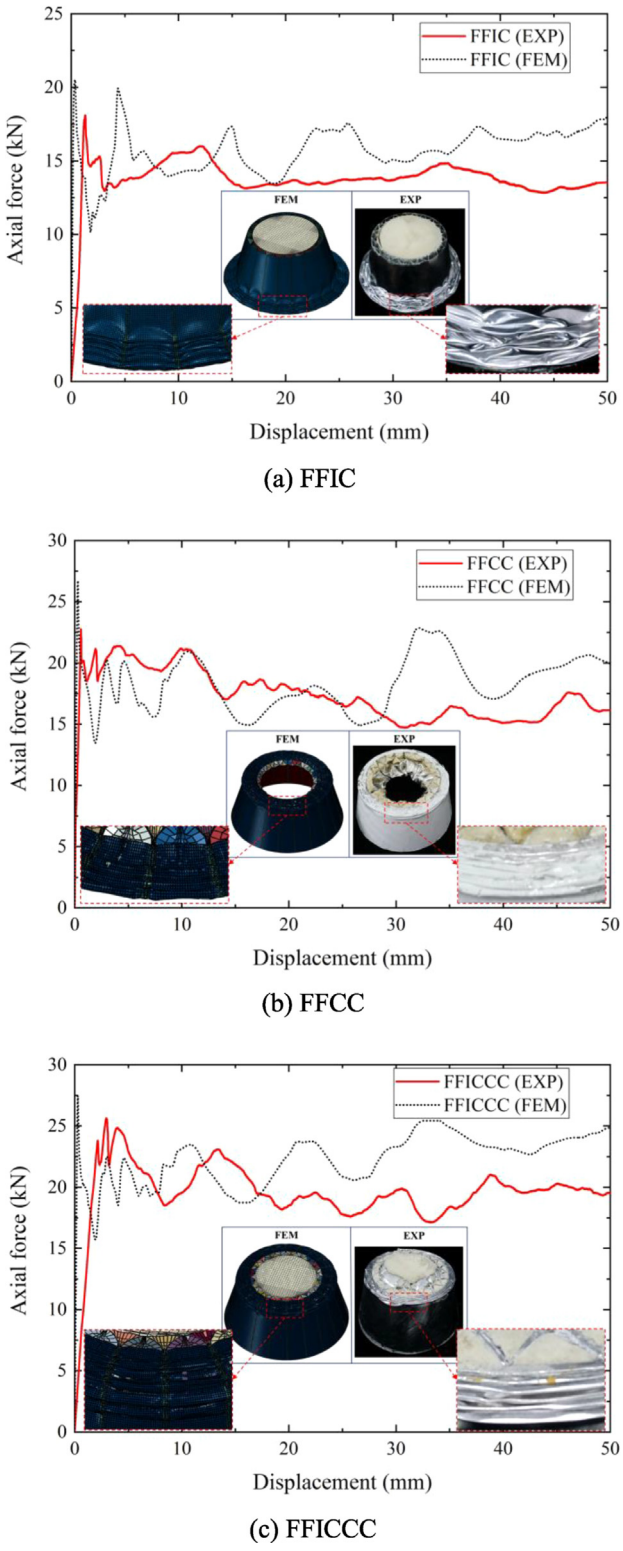

Fig. 9. Comparison of quasi-static axial compressive force versus displacement curve and deformation mode between FE simulation and experimental measurement: (a) FFIC, (b) FFCC and (c) FFICCC.

So, the measured initial stiffness was much lower than that calculated numerically, leading to the deformation delay of the experimental curve in Fig. 9. Correspondingly, at a specific compression distance, the energy absorption measured from experiment was consistently lower than that obtained from FE simulation.

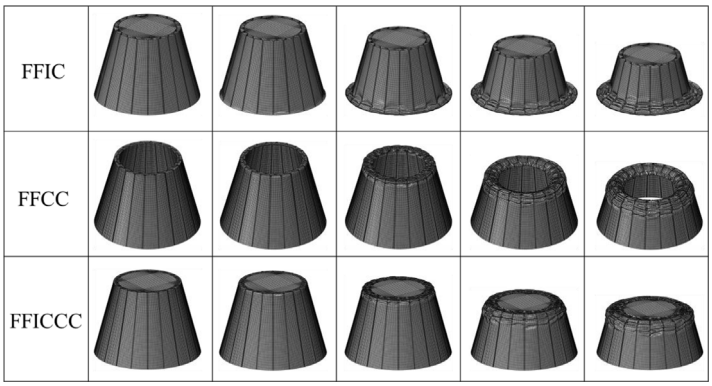

Fig. 10. Numerically simulated deformation mode of FFIC, FFCC and FFICCC with different crushing distances.

Table 3
Peak force (*PF*) and specific energy absorption (*SEA*): comparison between FE simulation and experimental measurement under quasi-static uniaxial compression.

Specimens		S-FFIC	S-FFCC	S-FFICCC
PF (kN)	Simulation	20.40	26.65	27.39
	Experiment	18.11	22.76	25.63
	Error	12.6%	17.1%	6.9%
EA (kJ)	Simulation	0.78	0.91	1.12
	Experiment	0.69	0.87	0.99
	Error	12.0%	4.6%	13.1%
SEA (kJ/kg)	Simulation	3.22	5.79	4.16
	Experiment	2.82	5.56	3.67
	Error	14.2%	4.1%	13.4%

3.3. Foam-shell interaction effect

It could be seen from Table 3 that the FFIC had the lowest *SEA* and *EA*, the FFICCC had the highest *EA*, while the FFCC had the highest *SEA*. This was mainly attributed to different deformation mechanisms. Fig. 10 showed the deformation modes of FFIC, FFCC and FFICCC with different crushing distances. It could be seen that the deformation always started at the ends of the structure, and the entire crushing process was accompanied with the formation of continuous folds. In fact, the formation of each fluctuation in the load versus deflection curve corresponds to the formation of one folds [41]. To further explore the influence mechanism of foam filling, cross-sectional views of the three foam-filled structures after deformation were illustrated in Fig. 11. It could be seen that, for the FFIC, there was almost no mutual interaction between the foam filler and the TCSS. Compared with the unfilled structure (i.e., the TCSS), the increase in *EA* was mainly due to energy absorption of the foam itself. However, due to the large internal space and corresponding increase in structural mass, the *SEA* of the structure decreased. In contrast, during the deformation process of the FFCC, the foam was squeezed into the gaps of adjacent plastic hinges of the metal shells, resulting in an obvious interaction between the PU foam and the metal shells. The *EA* of the structure was greatly improved with only a little mass increase, as the interstices of the sandwich core in which the foam fillers resided only took a small portion of the total structural volume. The corresponding increase in *SEA* was also significant. Such significant enhancement was barely obtained in alternative foam-filled energy-absorbers reported in previous studies, which can be attributed to the particularity of the TCSS. As for the FFICCC, its energy absorption characteristics were somewhere in between the FFIC and the FFCC.

To better understand the interaction effect induced by foam filling, the crashworthiness of a single TCSS and a single conical foam structure under axial compression were numerically calculated, with relevant force versus displacement curves obtained. Fig. 12 compared the results with those of the foam-filled structures (i.e., FFIC, FFCC, FFICCC).

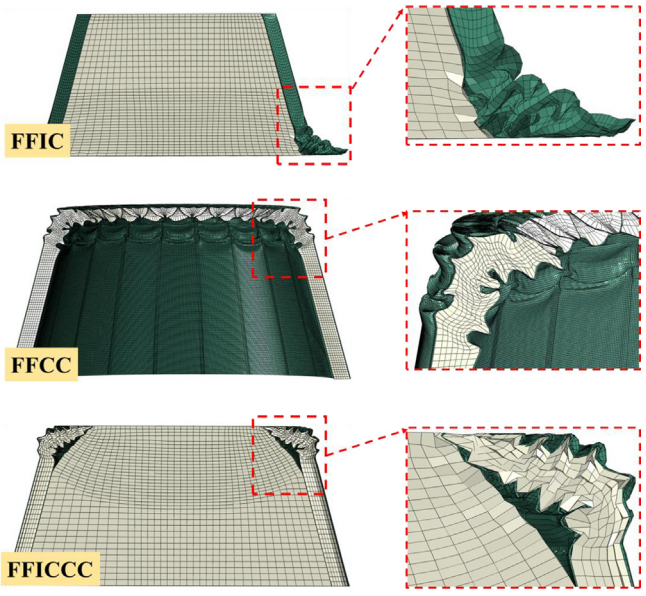

Fig. 11. Numerically simulated deformation mechanisms of FFIC, FFCC and FFICCC.

Note that the foam model was a conical structure, with its taper and height consistent with experimental specimens, and its mass equal to the mass of foam fillers in the corresponding foam-filled structure. It was seen that the stress versus strain curve of each foam-filled TCSS was higher than that of the TCSS + Foam, and the discrepancy was attributed to the interaction effect. The area under the curve of TCSS + Foam was almost the same as that under the curve of FFIC, as shown in Fig. 12(a). The *EA* of FFIC was basically a simple superposition of a single foam and a single TCSS, with almost no interaction effect. From Fig. 12(b), however, it could be seen that the area under the curve of FFCC was much larger than that under the curve of TCSS + Foam. This means that the energy absorption of FFCC was much larger than the simple superposition of a single foam and a single TCSS, as the interaction effect between foam and TCSS was strong in FFCC. Similar results were obtained for FFICCC, but the interaction effect was mainly due to foam fillers in the sandwich core, not those in the inner cavity, and hence its *SEA* was expected to be much smaller than that of FFCC.

Table 4 presented the values of *EA*, *Mass* and *SEA* for each constituent of the three foam-filled structures. The *EA* of a single foam exhibited the following trend: FFICCC > FFIC > FFCC, which was mainly determined by the mass of the foam. The mass of foam in a FFCC was much smaller than that in either FFIC or FFICCC. In addition, it could be seen from Table 4 that the *SEA* of single foam varied from

Table 4
Comparison of PU Foam, TCSS, and foam-filled TCSS.

		FFIC	FFCC	FFICCC
EA (kJ)	TCSS	0.60	0.60	0.60
	Foam	0.19	0.03	0.24
	TCSS+Foam	0.79	0.63	0.83
	Foam-filled TCSS	0.79	0.91	1.12
Mass (g)	TCSS	134.73	134.73	134.73
	Foam	110.39	24.54	134.93
	TCSS+Foam	245.12	159.27	269.66
	Foam-filled TCSS	245.12	159.27	269.66
SEA (kJ/kg)	TCSS	4.42	4.42	4.42
	Foam	1.72	1.22	1.75
	TCSS+Foam	3.20	3.92	3.08
	Foam-filled TCSS	3.20	5.74	4.16

1.72 via 1.22 to 1.75 kJ/kg, while that *SEA* of TCSS was 4.42 kJ/kg. Therefore, when the interaction effect was not obvious, simply filling the foam into TCSS would cause the *SEA* of the foam-filled structure lower than that of the TCSS. This was why the *SEA* of either FFIC or FFICCC was inferior to the TCSS. In the FFCC, the strong interaction effect between foam and TCSS and small increase in structural mass led to 30% increase in *SEA* relative to the TCSS.

4. Discussions

In this section, the influences of wall thickness (t), semi-apical angle (θ) and dynamic impact velocity on the crushing behaviors of three different foam-filled structures (i.e., FFIC, FFCC, and FFICCC) were quantified using FE simulations.

4.1. Effect of wall thickness

Fig. 13 displayed how the thickness (t) of face sheet and corrugation members affected the crashworthiness of foam-filled TCSS under quasi-static axial compression. It could be seen that when t was constant, the curve of FFICCC was higher than FFCC, and the curve of FFCC was higher than FFIC. The curves of FFIC, FFCC and FFICCC all increased with the increase of t. To further analyze the influence of the change in t on energy absorption characteristics, the *EA*, *SEA*, *PF* and *SEAV* of the foam-filled structures were calculated and compared with those of TCSS in Fig. 14.

It could be seen from Fig. 14(a) that the *EA* of TCSS, FFIC, FFCC and FFICCC all increased nearly linearly with the increase of t, and the four structures compared varied in the following order, $EA_{\mathrm{FFICCC}} > EA_{\mathrm{FFCC}} > EA_{\mathrm{FFIC}} > EA_{\mathrm{TCSS}}$. The results of from Fig. 14(b) showed that the *SEA* of TCSS, FFIC, FFCC and FFICCC all increased with the increase of t, but the increasing speed gradually slowed down, and the following order was obtained, $SEA_{\mathrm{FFCC}} > SEA_{\mathrm{FFICCC}} > SEA_{\mathrm{FFIC}}$. The *SEA* of FFCC was consistently higher than the TCSS, but its superiority gradually decreased with the increase of t because foam filling played an increasingly smaller role as t was increased. When t was relatively small (t = 0.2 or 0.4 mm), the *SEA* of FFICCC was equivalent to the TCSS. However, when t was enlarged (t = 0.6 or 0.8 mm), the *SEA* of FFICCC became smaller than the TCSS and, as t was further increased, the difference between the two structures also increased. The increase of t led to smaller *SEA* of FFICC relative to TCSS, because there was almost no interaction effect between the foam and TCSS and the mass of foam filling was large.

It could be seen from Fig. 14(c) that the *PF* of FFIC was almost equal to that of the TCSS and, as t was increased, the difference between the two diminished. This was mainly due to the low strength of foam compared to the metal structure (TCSS). In comparison, the *PF* of FFCC was consistently higher than that of either TCSS or FFIC, but this advantage gradually decreased as t was increased. The foam filled in the corrugated channel had a good support and interaction effect on the surrounding TCSS, which could effectively suppress the occurrence of initial buckling in FFCC. The *PF* of FFICCC was almost equal to that of FFCC over the entire range of t considered.

Since the change of t hardly changes the overall volume of the foam-filled structures considered, the variation trend of *SEAV* was consistent with that of *EA*, as shown in Fig. 14(d).

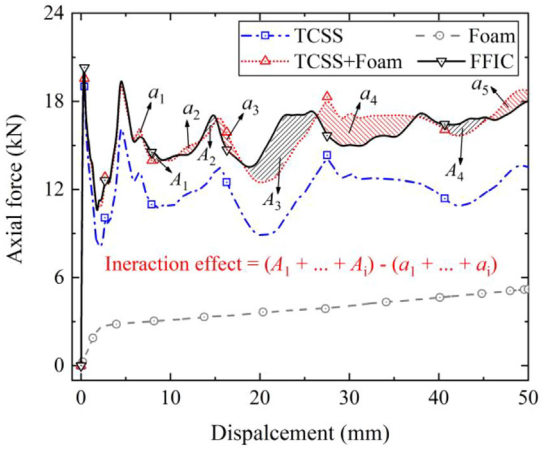

(a) FFIC

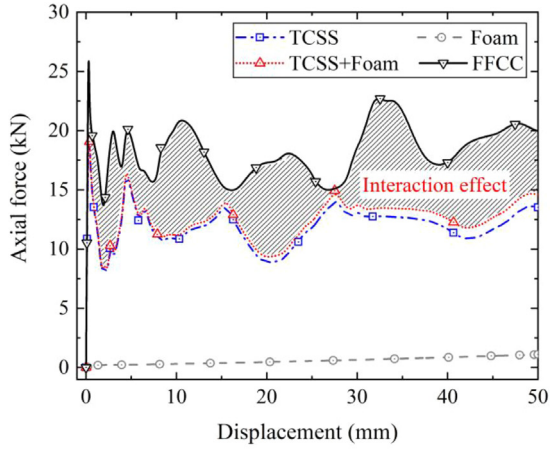

(b) FFCC

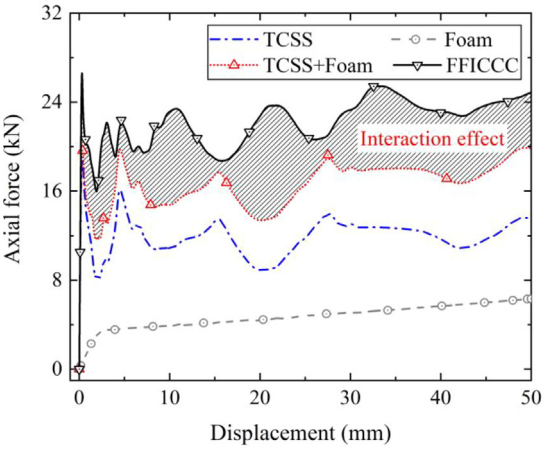

(c) FFICCC

Fig. 12. Force versus displacement curves of PU Foam, TCSS, and foam-filled TCSS: (a) FFIC, (b) FFCC and (c) FFICCC.

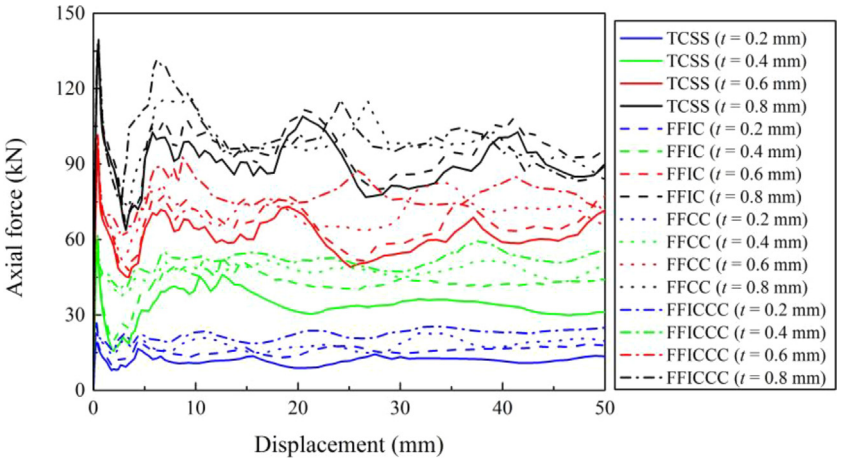

Fig. 13. Effect of thickness on force versus displacement curves.

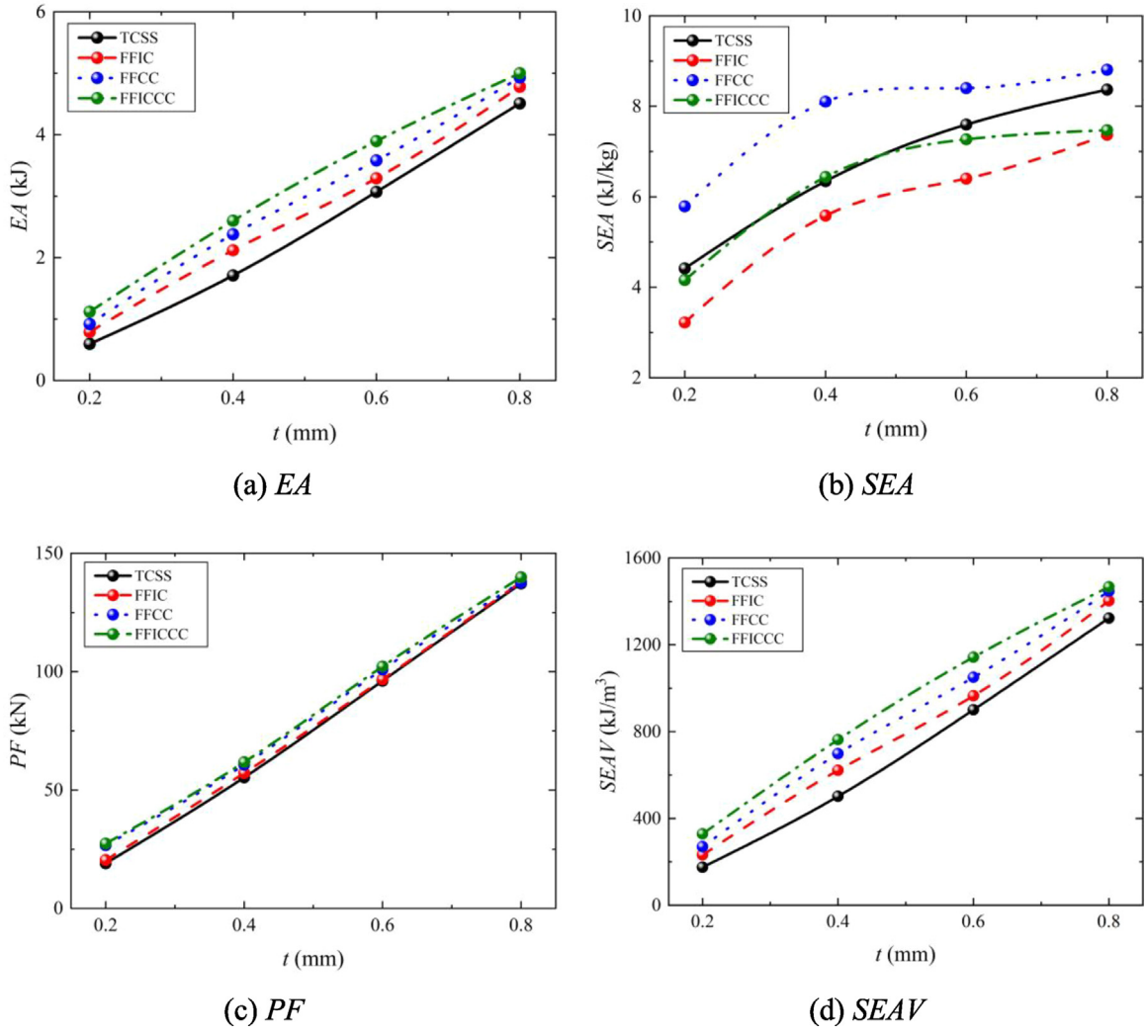

Fig. 14. Effect of thickness on *EA*, *SEA*, *PF* and *SEAV*.

4.2. Effect of semi-apical angle

To understand how the semi-apical angle (θ) affects the energy absorption characteristics of foam-filled TCSS, this section studied different structures: TCSS, FFIC, FFCC, FFICC. To fully reflect the influence of foam filling, the mass of the TCSS in foam-filled structures with different θ remained unchanged, equal to the mass of TCSS in experimental specimens (i.e., S-FFIC, S-FFCC, S-FFICCC). The results of

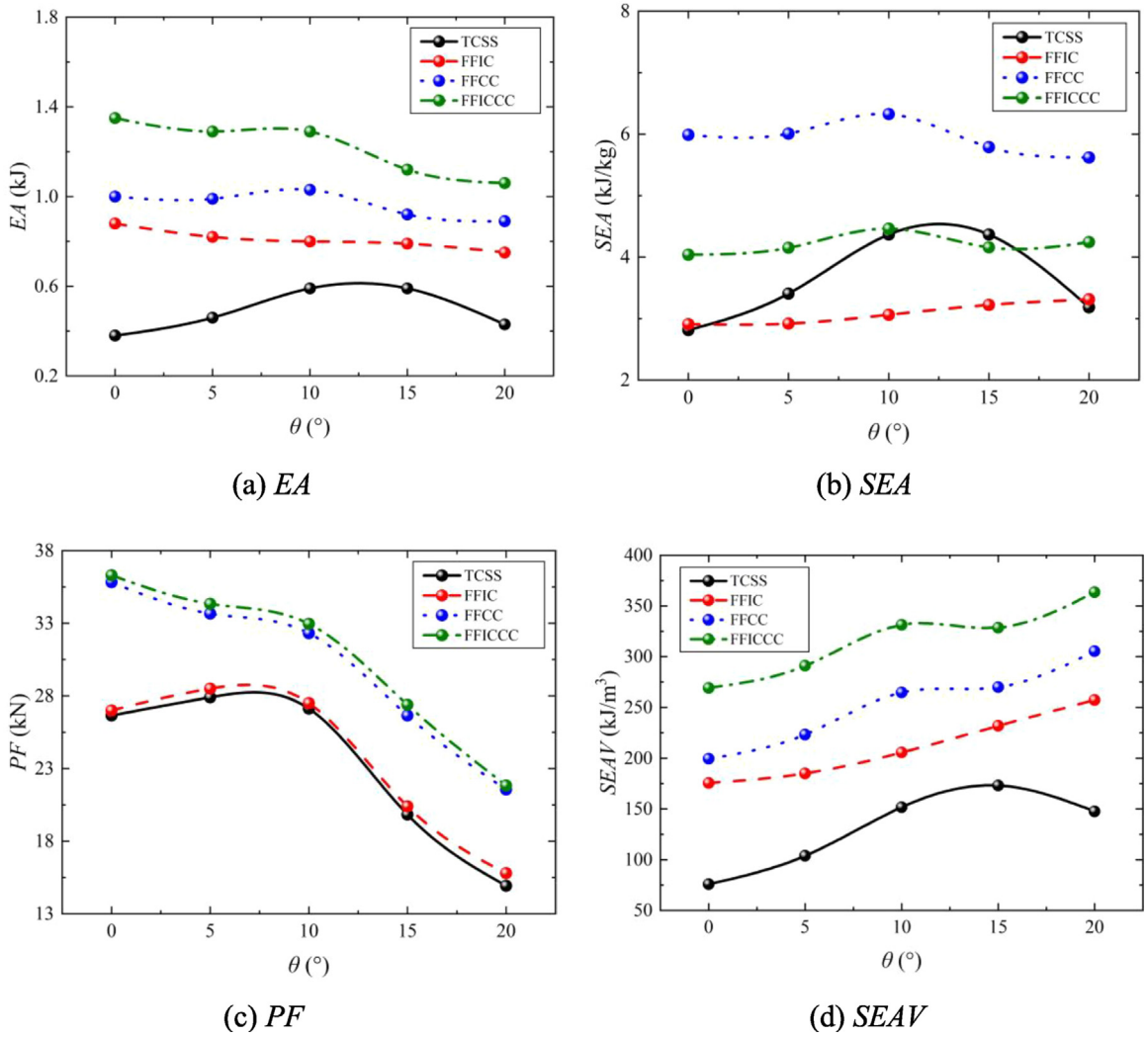

Fig. 15. Effect of semi-apical angle on *EA*, *SEA*, *PF* and *SEAV*.

EA, *SEA*, *PF* and *SEAV* obtained via FE simulations were presented in Fig. 15.

The results of Fig. 15(a) showed that the *EA* of TCSS first increases and then decreases with increasing θ, peaking when θ = 10°–15°. In contrast, varying θ had a relatively low influence on the *EA* of FFIC, FFCC and FFICCC which, overall, decreases slightly with the increase of θ. With the semi-apical angle fixed, it was seen from Fig. 15(a) that $EA_{\mathrm{FFICCC}} > EA_{\mathrm{FFCC}} > EA_{\mathrm{FFIC}} > EA_{\mathrm{TCSS}}$. However, the results presented in Fig. 15(b) demonstrated that the *SEA* of foam-filled structures was ranked as: $SEA_{\mathrm{FFCC}} > SEA_{\mathrm{FFICCC}} > SEA_{\mathrm{FFIC}}$. In addition, the *SEA* of FFCC was higher than that of TCSS at each θ. The *SEA* of FFICCC was less than that of TCSS when θ = 15°, but greater at other values of θ and, when θ = 0° or 20°, the *SEA* of TCSS differed most from that of FFICCC. When θ = 0° or 20°, the *SEA* of FFIC was similar to that of TCSS, but smaller at other θ; when θ = 10°–15°, the *SEA* of TCSS differed most from that of FFIC. Similar to the case of *EA*, with the increase of θ, the *SEA* of TCSS increases at first and then decreases, peaking when θ = 10°–15°. The *SEA* of FFIC gradually increases with the increase of θ. In contrast, with the increase of θ, the *SEA* of FFCC and FFICCC both increases at first and then decreases, peaking when θ = 10°.

It could be seen from Fig. 15(c) that, with the value of θ fixed, the *PF* of the structures varied as: $PF_{\mathrm{FFICCC}} > PF_{\mathrm{FFCC}} > PF_{\mathrm{FFIC}} > PF_{\mathrm{TCSS}}$. The *PF* of FFICCC was relatively close to the FFCC, while the *PF* of FFIC was relatively close to the TCSS. The *PF* of either FFIC or TCSS remained almost unchanged with the increase of θ, and gradually decreased when θ was greater than 10°. The *PF* of FFICCC and FFFCC gradually decreased as θ was increased.

The results presented in Fig. 15(d) revealed that $SEAV_{\mathrm{FFICCC}} > SEAV_{\mathrm{FFCC}} > SEAV_{\mathrm{FFIC}} > SEAV_{\mathrm{TCSS}}$. The *SEAV* of FFIC, FFCC, and FFICCC all increased with the increase of θ, which was mainly because the volume of the structure decreased with increasing θ. As θ was increased, the *SEAV* of TCSS increased at first and then decreased, reaching a maximum at θ = 15°.

4.3. Dynamic loading

Energy absorbing structures often experience dynamic impact loads, so it is important to study their dynamic responses under such loading. In the current study, to represent the behavior of both metal and foam materials under dynamic loading, the following relationship was used:

$$\dot{\varepsilon} = D\left(\frac{\sigma_{\mathrm{d}}}{\sigma_{\mathrm{s}}} - 1\right)^{\mathrm{m}} \tag{4}$$

where σ_{s} and σ_{d} denote the quasi-static and dynamic yield stresses, and D and m are dynamic constants. For the aluminum alloy (1060Al) and PU foam considered here, relevant parameters were listed in Table 5 [26].

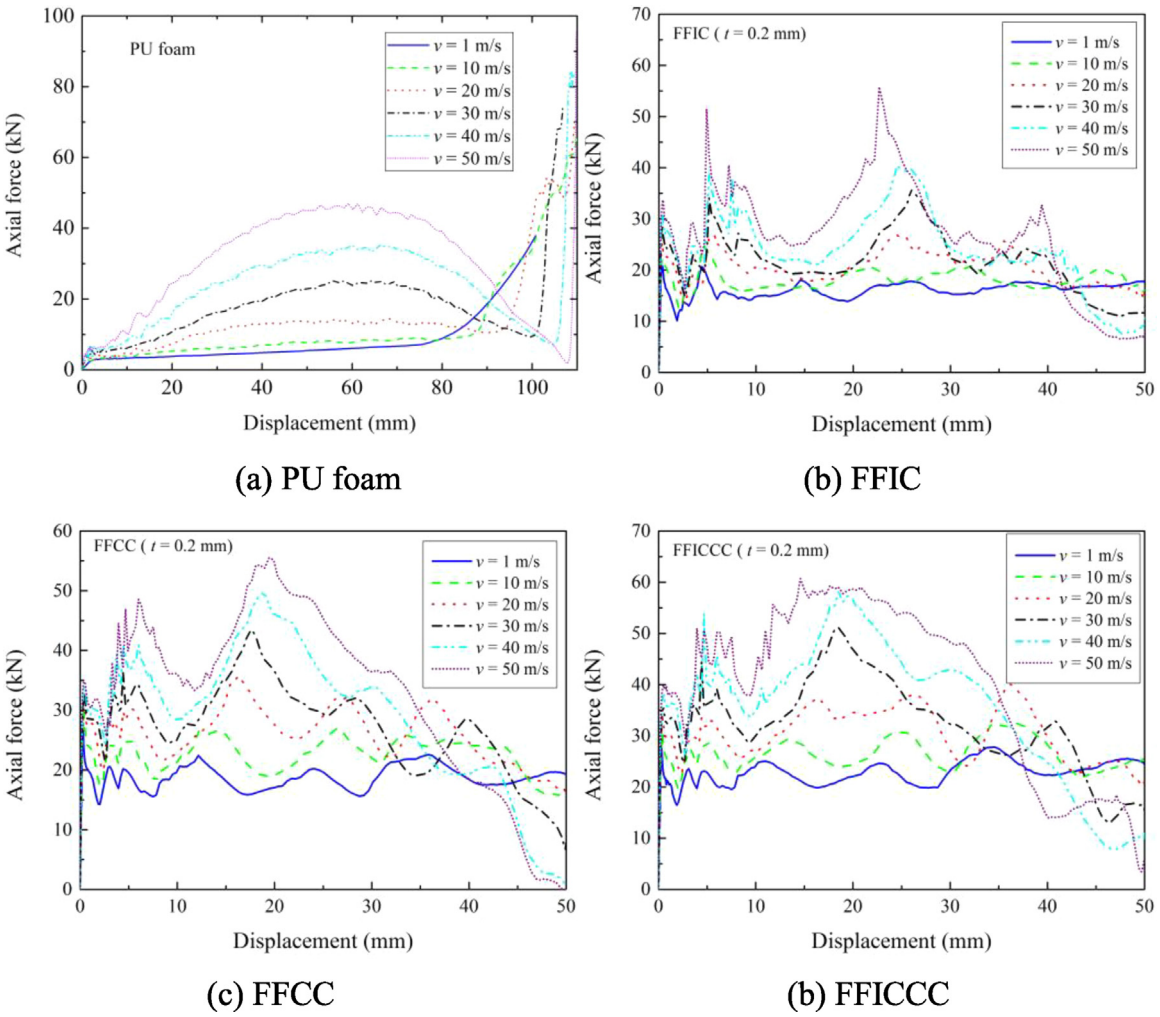

Fig. 16. Effect of impact velocity on force versus displacement curve of foam-filled structure: (a) PU foam, (b) FFIC, (c) FFCC and (d) FFICCC.

Table 5
Dynamic material parameters of Al and PU foam [26].

Material	D (s^{-1})	m
Aluminum 1060Al	1 288 000	4
PU foam	4638	2.285

To investigate the influence of impact velocity (v), only the loading velocity was changed in the FE model, the geometric size of the structure was consistent with the size of the experimental specimens, as Fig. 1 and Table 1, and the crushing distance was 50 mm. The force versus displacement curves of PU foam, FFIC, FFCC and FFICCC for selected values of v thus calculated were displayed in Fig. 16. The axial force of PU foam increased as v was increased. And the axial force of a foam-filled conical structure increased as v was increased, regardless of foam filling type. As v was increased, the maximum axial force may exceed the initial peak force. Consequently, for unified comparison, the initial peak force was selected in subsequent data analysis. From Fig. 17 it was seen that the *PF* of FFIC, FFCC and FFICCC all increased linearly with increasing v, with nearly the same variation trend. Similar conclusions held for the *SEA* of foam-filled structures, as shown in Fig. 17.

5. Concluding remarks

The energy absorption characteristics of three different foam-filled truncated conical sandwich shells with corrugated cores, i.e., foam filling inner cavity (FFIC), foam filling corrugated channel (FFCC) and foam filling inner cavity and corrugated channel (FFICCC), were systematically investigated, both experimentally and numerically. Influences of wall thickness, semi-apical angle and loading speed on key crashworthiness parameters (*EA*, *SEA*, *PF* and *SEAV*) were quantified. Main findings were summarized as follows:

1. The Energy absorption (*EA*) of foam-filled structures (FFIC, FFCC, FFICCC) was higher than that their unfilled counterpart (i.e., TCSS).

2. The specific energy absorption (*SEA*) was affected by the foam filling method, and not all foam-filled TCSS showed obvious strengthening effect. Only for the case of foam filling corrugated channel (i.e., the FFCC), the interaction effect between foam and metallic shells was most obvious, thus contributing to the highest *SEA*.

3. With increasing wall thickness, the *EA*, *SEA*, *PF* and *SEAV* of all foam-filled structures increased, but the difference among FFIC, FFCC and FFICCC gradually decreased.

4. Both the *EA* and *SEA* of foam-filled structures first increased and then decreased as the semi-apical angle was increased, peaking at $\theta = 10°\sim15°$. Compared with the unfilled TCSS, the foam-filled TCSS exhibited obvious superiority in energy absorption especially at $\theta = 0°$ or 20°. Moreover, foam filling could efficiently increase the *SEAV*, with performance ranked as: $SEAV_{\mathrm{FFICCC}} > SEAV_{\mathrm{FFCC}} > SEAV_{\mathrm{FFIC}} > SEAV_{\mathrm{TCSS}}$.

5. The *PF* and *SEA* of FFIC, FFCC and FFICCC all increased linearly with impact velocity.

The results of the present study provide useful guidance for designing energy absorbing structures with superior crashworthiness.

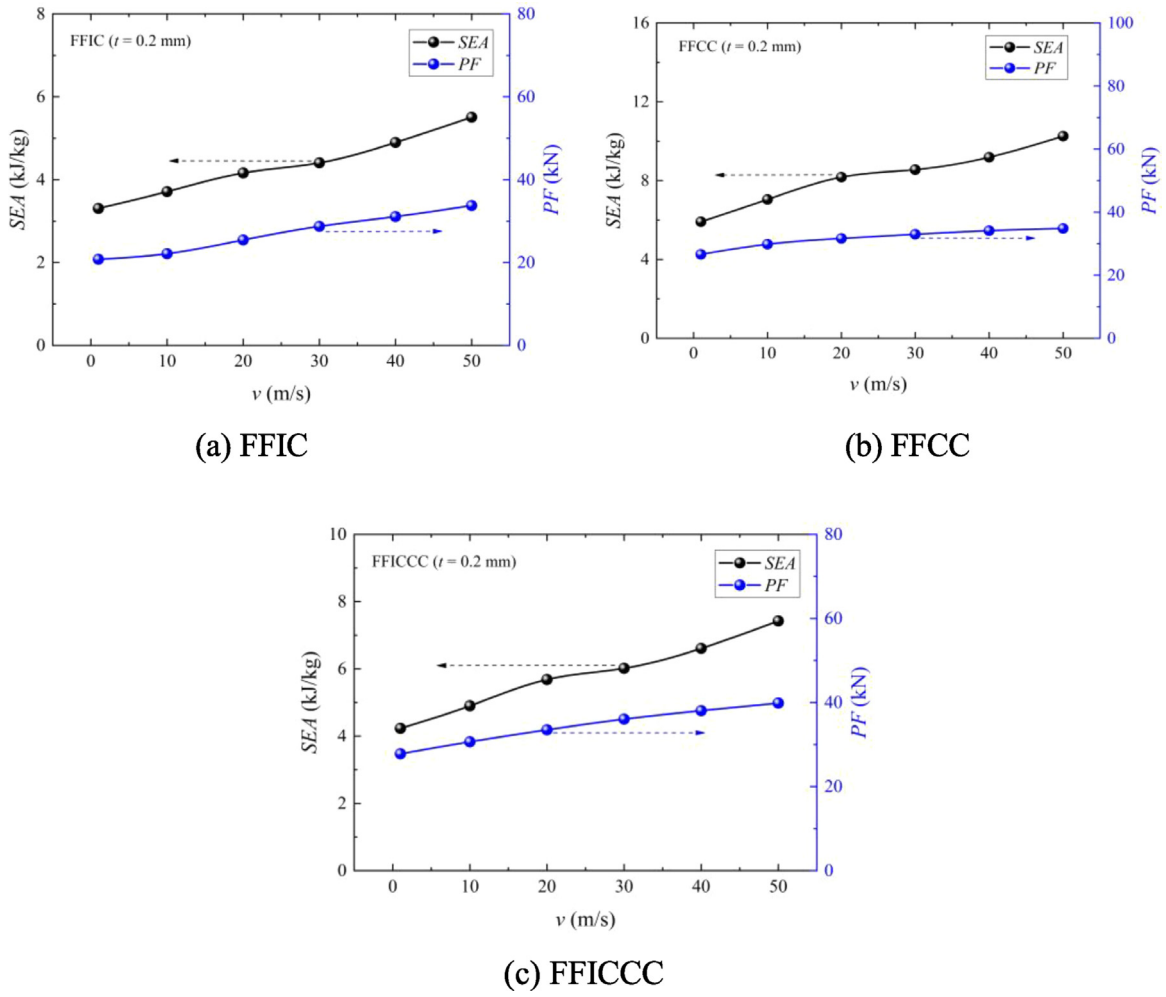

Fig. 17. Effect of impact velocity on *PF* and *SEA* of foam-filled structure: (a) FFIC, (b) FFCC and (c) FFICC.

CRediT authorship contribution statement

Mao Yang: Writing – review & editing, Writing – original draft, Visualization, Validation, Project administration, Methodology, Investigation, Formal analysis, Data curation, Conceptualization. **Bin Han:** Writing – review & editing, Supervision, Resources, Project administration. **Yongjian Mao:** Resources. **Jun Zhang:** Resources. **Tian Jian Lu:** Writing – review & editing, Supervision, Resources, Project administration, Funding acquisition.

Declaration of competing interest

The authors declare that they have no known competing financial interests or personal relationships that could have appeared to influence the work reported in this paper.

Data availability

No data was used for the research described in the article.

Acknowledgments

This work was supported by the National Natural Science Foundation of China (11802221, 51875441, 11972185, 12032010, 12072334, 11602256).

References

[1] R.H. Zhang, Z.C. He, H.W. Wang, F. You, K.N. Li, Study on self-tuning tyre friction control for developing main-servo loop integrated chassis control system, IEEE Access 5 (2017) 6649–6660.
[2] R. Shams, A. Niknejad, A.G. Olabi, M.Z. Nejad, Quasi-static flattening energy absorption process on preformed circular tubes by numerical and experimental analyses, Thin Walled Struct. 144 (2019) 106260.
[3] H. Hatami, M.S. Rad, A.G. Jahromi, A theoretical analysis of the energy absorption response of expanded metal tubes under impact loads, Int. J. Impact Eng. 109 (2017) 224–239.
[4] K.A. Praveen, M.N. Mohamed, A. Jusuf, T. Dirgantara, L. Gunawan, Axial crash performance of press-formed open and end-capped cylindrical tubes-A comparative analysis, Thin Walled Struct. 124 (2018) 468–488.
[5] Z. Fan, G. Lu, T.X. Yu, K. Liu, Axial crushing of triangular tubes, Int. J. Appl. Mech. 5 (2013) 1350008.
[6] T.N. Tran, T.N.T. Ton, Lateral crushing behaviour and theoretical prediction of thin walled rectangular and square tubes, Compos. Struct. 154 (2016) 374–384.
[7] A. Malekshahi, K.H. Shirazi, M. Shishehsaz, Axial crushing of prismatic multi-corner metal columns considering plastic hardening and curvature, J. Mech. 35 (2018) 1–12.
[8] S. Reddy, M. Abbasi, M. Fard, Multi-cornered thin-walled sheet metal members for enhanced crashworthiness and occupant protection, Thin Walled Struct. 94 (2015) 56–66.
[9] A. Baroutaji, M. Sajjia, A.G. Olabi, On the crashworthiness performance of thin walled energy absorbers: recent advances and future developments, Thin Walled Struct. 118 (2017) 137–163.
[10] G.M. Nagel, D.P. Thambiratnam, A numerical study on the impact response and energy absorption of tapered thin-walled tubes, Int. J. Mech. Sci. 46 (2004) 201–216.

[11] X. Zhang, H. Zhang, Axial crushing of circular multi-cell columns, Int. J. Impact Eng. 65 (2014) 110–125.
[12] Y. Zhang, J. Wang, C. Wang, Y. Zeng, T. Chen, Crashworthiness of bionic fractal hierarchical structures, Mater. Des. 158 (2018) 147–159.
[13] A. Alavi Nia, M. Parsapour, Comparative analysis of energy absorption capacity of simple and multi-cell thin-walled tubes with triangular, square, hexagonal and octagonal sections, Thin Walled Struct. 74 (2014) 155–165.
[14] F. Xiong, D. Wang, S. Yin, Optimization analysis of novel foam-filled elliptical columns under multiple oblique impact loading, Mater. Des. 156 (2018) 198–214.
[15] H. Saeidi Googarchin, M. Pasandidehpoor, A. Mahmoodi, M.H. Shojaeefard, Energy absorption analysis for tapered multi-cell tubes improved by foams: theoretical development and numerical simulation, Compos. Struct. 207 (2019) 213–222.
[16] I. Duarte, L. Krstulović-Opara, J. Dias-de-Oliveira, M. Vesenjak, Axial crush performance of polymer-aluminium alloy hybrid foam filled tubes, Thin Walled Struct. 138 (2019) 124–136.
[17] I. Duarte, M. Vesenjak, L. Krstulović-Opara, I. Anžel, J.M. Ferreira, Manufacturing and bending behaviour of in situ foam-filled aluminium alloy tubes, Mater. Des. 66 (2015) 532–544.
[18] J. Banhart, Manufacture, characterisation and application of cellular metals and metal foams, Prog. Mater. Sci. 46 (2001) 559–632.
[19] M.F. Ashby, T. Evans, N.A. Fleck, J.W. Hutchinson, H.N.G. Wadley, L.J. Gibson, Metal Foams: A Design Guide, Elsevier, 2000.
[20] S.C. Pinto, P.A. Marques, M. Vesenjak, R. Vicente, L. Godinho, L. Krstulović-Opara, I. Duarte, Characterization and physical properties of aluminium foam–polydimethylsiloxane nanocomposite hybrid structures, Compos. Struct. 230 (2019) 111521.
[21] M. Vesenjak, I. Duarte, J. Baumeister, H. Göhler, L. Krstulović-Opara, Ren Z., Bending performance evaluation of aluminium alloy tubes filled with different cellular metal cores, Compos. Struct. 234 (2020) 111748.
[22] I. Duarte, M. Vesenjak, L. Krstulović-Opara, Z. Ren, Compressive performance evaluation of APM (Advanced Pore Morphology) foam filled tubes, Compos. Struct. 134 (2015) 409–420.
[23] I. Duarte, M. Vesenjak, L. Krstulović-Opara, Z. Ren, Crush performance of multifunctional hybrid foams based on an aluminium alloy open-cell foam skeleton, Polym. Test. 67 (2018) 246–256.
[24] I. Duarte, L. Krstulović-Opara, M. Vesenjak, Axial crush behaviour of the aluminium alloy in-situ foam filled tubes with very low wall thickness, Compos. Struct. 192 (2018) 184–192.
[25] S.C. Pinto, P.A. Marques, R. Vicente, L. Godinho, I. Duarte, Hybrid structures made of polyurethane/graphene nanocomposite foams embedded within aluminum open-cell foam, Metals 10 (2020) 768.
[26] S. Azarakhsh, A. Ghamarian, Collapse behavior of thin-walled conical tube clamped at both ends subjected to axial and oblique loads, Thin Walled Struct. 112 (2017) 1–11.
[27] M. Mahbod, M. Asgari, Energy absorption analysis of a novel foam-filled corrugated composite tube under axial and oblique loadings, Thin Walled Struct. 129 (2018) 58–73.
[28] R. Yao, Z. Zhao, W. Hao, G. Yin, B. Zhang, Experimental and theoretical investigations on axial crushing of aluminum foam-filled grooved tube, Compos. Struct. 226 (2019) 111229.
[29] M. Altin, E. Acar, M.A. Güler, Foam filling options for crashworthiness optimization of thin-walled multi-tubular circular columns, Thin Walled Struct. 131 (2018) 309–323.
[30] Q. Liu, J. Fu, J. Wang, J. Ma, H. Chen, Q. Li, D. Hui, Axial and lateral crushing responses of aluminum honeycombs filled with EPP foam, Composites B 130 (2017) 236–247.
[31] A.G. Evans, J.W. Hutchinson, N.A. Fleck, M.F. Ashby, H.N.G. Wadley, The topological design of multifunctional cellular metals, Prog. Mater. Sci. 46 (2001) 309–327.
[32] F. Côté, V.S. Deshpande, N.A. Fleck, A.G. Evans, The compressive and shear responses of corrugated and diamond lattice materials, Int. J. Solids Struct. 43 (2006) 6220–6242.
[33] W. Wang, X. Yang, B. Han, Q.C. Zhang, X.F. Wang, T.J. Lu, Analytical design of effective thermal conductivity for fluid-saturated prismatic cellular metal honeycombs, Theor. Appl. Mech. Lett. 6 (2016) 69–75.
[34] L.L. Yan, B. Yu, B. Han, Q.C. Zhang, T.J. Lu, B.H. Lu, Effects of aluminum foam filling on the low-velocity impact response of sandwich panels with corrugated cores, J. Sandw. Struct. Mater. 22 (2020) 929–947.
[35] B. Han, K.K. Qin, B. Yu, Q.C. Zhang, C.Q. Chen, T.J. Lu, Design optimization of foam-reinforced corrugated sandwich beams, Compos. Struct. 130 (2015) 51–62.
[36] B. Yu, B. Han, C.Y. Ni, Q.C. Zhang, C.Q. Chen, T.J. Lu, Dynamic crushing of all-metallic corrugated panels filled with close-celled aluminum foams, Int. J. Appl. Mech. 82 (2015) 011006.
[37] B. Han, K.K. Qin, B. Yu, B. Wang, Q.C. Zhang, T.J. Lu, Honeycomb-corrugation hybrid as a novel sandwich core for significantly enhanced compressive performance, Mater. Des. 93 (2016) 271–282.
[38] X. Wang, R.P. Yu, Q.C. Zhang, L. Li, X. Li, Z.Y. Zhao, B. Han, S.Y. He, T.J. Lu, Dynamic response of clamped sandwich beams with fluid-fillied corrugated cores, Int. J. Impact Eng. 139 (2020) 103533.
[39] R.P. Yu, X. Wang, Q.C. Zhang, L. Li, S.Y. He, B. Han, C.Y. Ni, Z.Y. Zhao, T.J. Lu, Effects of sand filling on the dynamic response of corrugated core sandwich beams under foam projectile impact, Composites B (2020) 108135.
[40] Z.N. Zhao, B. Han, F.H. Li, R. Zhang, P.B. Su, M. Yang, Q. Zhang, Q.C. Zhang, T.J. Lu, Enhanced bi-layer mosaic armor: experiments and simulation, Ceram. Int. 46 (2020) 23854–23866.
[41] M. Yang, B. Han, P.B. Su, Z.H. Wei, Q. Zhang, Q.C. Zhang, T.J. Lu, Axial crushing of ultralight all-metallic truncated conical sandwich shells with corrugated cores, Thin Walled Struct. 140 (2019) 318–330.
[42] M. Yang, B. Han, P.B. Su, Z.H. Wei, Q. Zhang, Q.C. Zhang, T.J. Lu, Free vibration and axial compression of all-metallic cylindrical and truncated conical sandwich shells with corrugated cores, J. Sandw. Struct. Mater. (2020) 1099636220909792.
[43] M. Yang, B. Han, P.B. Su, F.H. Li, Z.N. Zhao, Q. Zhang, Q.C. Zhang, Z.J. Hong, T.J. Lu, Oblique crushing of truncated conical sandwich shell with corrugated core, Mech. Adv. Mater. Struct. (2020) 1–14.
[44] M. Yang, B. Han, P.B. Su, Q. Zhang, Q.C. Zhang, Z.Y. Zhao, C.Y. Ni, T.J. Lu, Crashworthiness of hierarchical truncated conical shells with corrugated cores, Int. J. Mech. Sci. (2020) 106171.
[45] N. San Ha, G. Lu, Thin-walled corrugated structures: A review of crashworthiness designs and energy absorption characteristics, Thin Walled Struct. 157 (2020) 106995.
[46] A. Ghamarian, M.T. Abadi, Axial crushing analysis of end-capped circular tubes, Thin Walled Struct. 49 (2011) 743–752.
[47] J. Fang, Y. Gao, X. An, G. Sun, J. Chen, Q. Li, Design of transversely-graded foam and wall thickness structures for crashworthiness criteria, Composites B 92 (2016) 338–349.
[48] T. Belytschko, J.I. Lin, C.S. Tsay, Explicit algorithms for the nonlinear dynamics of shells, Comput. Methods Appl. Mech. Engrg. 42 (1984) 225–251.